Bachelor of Science Thesis
Department of Physics
Particle and Nuclear Physics Division

# Degradation Studies of $LaBr_3$ Detector Units in High-Radiation Scenarios for Nuclear Fuel Inspection

*Author*
Anton Nordin
*Supervisor*
Pavel Golubev
*Co-Supervisor*
Linus Ros


Examination fall 2025. 15HP, half-pace
Presented June 13, 2025

# Abstract

Nondestructive assaying (NDA) is an important step in ensuring the safe handling of spent nuclear fuel and radioactive waste. The assaying techniques require the use of ionizing radiation detectors to determine the activity of said fuel. One candidate detector for such use is the cerium-activated $LaBr_3$ inorganic crystal scintillator. This scintillator offers excellent resolution, decay times and light yield, making for an excellent scintillator detector. During NDA the detector will be exposed to large doses of radiation. To establish whether the detector is a good candidate or not, it is important to investigate how the detector holds up against these large doses and to what degree they cause degradation of its scintillation qualities.

In this thesis a comparison is done between three different crystal scintillators; a LaBr-scintillator irradiated with 9.8 kGy in $\gamma$- and neutron radiation, a NaI(Tl)-scintillator and a reference undamaged LaBr-scintillator. By measuring the main peaks of $^{137}$Cs, $^{22}$Na and $^{60}$Co and calculating the resolution of these peaks, the degradation in resolution and Fano factor in LaBr $\gamma$-detection units due to large doses of radiation are discussed.

The study measures 6.193(1)% resolution peaks at 661.7 keV using the irradiated LaBr-scintillator, compared to a resolution of 3.260(1)% using the undamaged LaBr. The average relative degradation in resolution across all the measured $\gamma$ energies measured to 74.1% with the peak for $^{60}$Co measuring as high as a 92.3(13)% degradation. Despite the high dose of radiation incurred, the irradiated LaBr still outperforms the NaI(Tl)-scintillator in terms of energy resolution.

The results presented in this thesis may serve as a guide in determining how reliable the LaBr-scintillator is in use for high-radiation scenarios, as well as valuable data for improving detector performance simulation is such scenarios. Further characterization to determine the degradation of light yield and how the crystal structure is affected by the heating and cooling during the irradiation process in future studies would give greater insight of the radiation hardness of the LaBr-scintillator. Its use in NDA may be limited to scenarios with smaller effective doses to ensure the longevity of the detector.

# Acknowledgements

I would like to thank first and foremost my supervisor Pavel, for spending his time teaching me about detectors and helping me during the many troubleshooting sessions when nothing seemed to work. Thanks to my co-supervisor Linus, who taught me plenty of things over our communications. I would also give thanks to the members of Lund University's Nuclear Structure Group, for being incredibly welcoming and supplying plenty of cake during meetings. Special acknowledgments to my peers also doing their thesis' with NSG for helping me perfecting a draft and moral support sharing an office. Additional thanks to Yuliia for many constructive comments on my work, helping me improve my writing, and Pico for organizing the writing workshops where i could bring questions to niche to google about my writing.

# Commonly used abbreviations

- STE - Self trapped exciton
- PD - Photodiode
- APD - Avalanche photodiode
- SiPM - Silicon Photomultiplier
- PMT - Photomultiplier tube
- ADC - Analog-to-digital converter
- MCA - Multichannel Analyzer
- FWHM - Full width half maximum
- NDA - Nondestructive assaying
- EMI - Electromagnetic interference

# Contents

# 1 Introduction

To establish safe protocols in handling nuclear fuel, one has to employ techniques to measure and calculate the remaining inventory of radioactive nuclei and the decay heat of the fuel. The nondestructive assaying techniques that allow for these measurements require detectors capable of generating a linear response to incoming ionizing radiation. One such candidate is the cerium-activated lanthanum bromide scintillator crystal $LaBr_3(Ce)$, which offers fast decay times, good energy resolution and fast counting rate capabilities.

In high-radiation scenarios, exposed material may undergo changes. In this thesis a LaBr-scintillator crystal that has been exposed to 9.8 kGy of neutron- and $\gamma$ radiation, will be characterized and compared to an undamaged LaBr- and a NaI(Tl)-scintillator crystal in order to determine if and to what degree irradiation has caused degradation of the scintillation properties of the crystal. This is done to determine whether the LaBr-scintillator detector is a qualified candidate for use in nondestructive-assaying in nuclear fuel inspection and other high-radiation scenarios that require fast and efficient $\gamma$ detectors, taking into account the high market cost of the LaBr-scintillator material.

This thesis will briefly introduce the phenomena of $\gamma$-radiation and how it interacts with matter before discussing the scintillator detector with a focus on the inorganic crystal scintillator LaBr. The different components necessary to acquire readable signals and build a $\gamma$ spectra are introduced and the measurement process is discussed. Finally, the results of the measurements are presented together with a discussion on the effects of irradiation on the LaBr scintillator.

# 2 $\gamma$ radiation

During nuclear decays such as $\alpha$- or $\beta$ decay, the resulting nucleus often has excess energy and is left in an excited state. The discharge of this excess energy as the nucleus decays back to the stable ground state takes the form of $\gamma$ radiation. $\gamma$ decay takes the form of electromagnetic radiation, with wavelengths typically much shorter than those of visible light. There are many different ways that $\gamma$-rays interact with matter, but in the case of radiation measurements; three interaction mechanisms dominate.

## 2.1 Charged particle interactions

$\gamma$ rays interact with matter mainly in three different ways, each dominating at a certain energy range depending on the material as illustrated in Figure 1. The intensity of $\gamma$ radiation as it interacts with material of thickness $\ell$ and linear attenuation constant $\mu_\ell$, is

attenuated with

$$I = I_0 e^{-\mu_\ell x}, \tag{1}$$

where $I_0$ is the initial intensity of the $\gamma$ ray. The attenuation constant is dependent on the material, whereas the interaction behind this attenuation constant is dependent on the energy of the incoming $\gamma$.

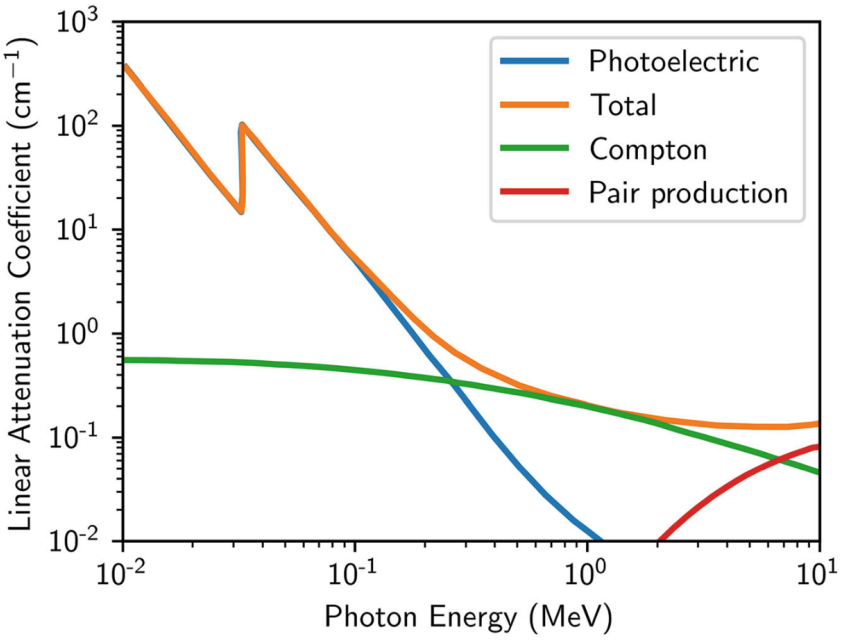


Figure 1: Plot showing the the linear attenuation coefficient of NaI as a function of photon energy. Taken from [1]

### 2.1.1 Photoelectric absorption

In this process, the photon interacts with an electron in an absorber atom, getting fully absorbed. The energy of the photon causes an electron to be ejected from this absorber. The energy of the ejected photoelectron is given by the difference in energy of the interacting photon and the binding energy of the electron in the absorber atom shell

$$E_{e^-} = h\nu - E_b. \tag{2}$$

Because an electron is ejected from the absorber atom, it leaves the absorber ionized. If this ejection is from a inner shell, there is a possibility for secondary photon emissions, X-rays, due to outer electrons filling a vacancy. As seen in Figure 1 this interaction is highly dominant at low- to mid photon energies in the $10^{-2}$ to $10^{-1}$ MeV range.

### 2.1.2 Compton scattering

Dominating interaction for the energy range of 1 to 10 MeV is Compton scattering. Incident photons interact with electrons in the material partially transferring its energy in a

scattering process. The electron becomes a free electron within the material with energy $E_e = E_\gamma - E_{B.E}$ corresponding to that of the energy lost by the photon in the process minus the binding energy of the electron. The scattered photon then continues to Compton scatter off of the electrons in the material until the photoelectric interaction takes precedent. The partial deposition of energy gives rise to specific spectral features as seen in Figure 2.

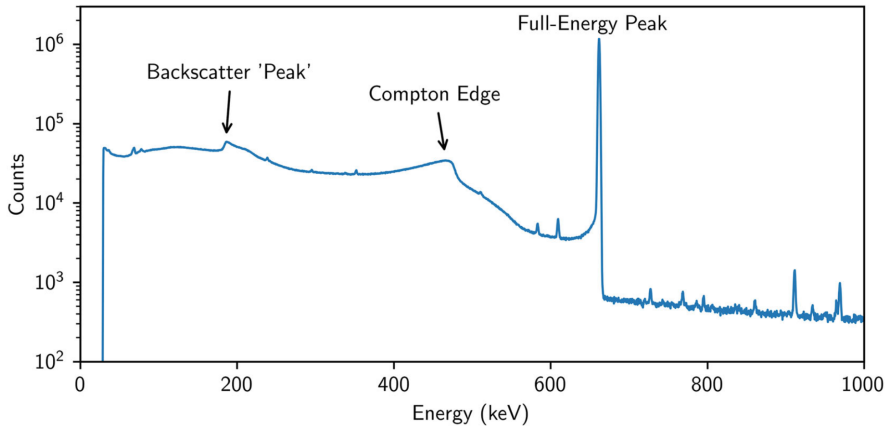


Figure 2: Spectrum of $^{137}$Cs showing the different spectroscopic features of Compton scattering, which are further discussed in the text. Plot is taken from [1]

The most prominent feature is the full-energy peak, when the complete energy of the photon is deposited in the sensitive volume of the detector, by any of the three interactions. At a slightly lower energy is the Compton edge: This energy is the maximum possible energy that a can be deposited in a single Compton-scattering event. Following this the photon escapes the detector with the rest of its energy. At even lower energies the photon scatter events for any recoil angle between 0-180°, followed by an escape, form the Compton continuum. On the lower extrema of these Compton features is the slight peak towards the lower end of energies. This is the backscatter peak, which corresponds to the photon undergoing scattering at around 180° in the material surrounding the detector, followed by a full deposition of the remaining photon energy in the actual detector.

### 2.1.3 Pair-production

As the energy of an incident photon exceeds the mass of two electrons, at around 1022 keV, a third mechanism becomes possible. Pair-production is when the photon is converted into an electron-positron pair. The electron and positron slow down within the material. The positron eventually annihilates with another electron in the material, producing two photons. These photons are of lower energy and are either absorbed in the material by the other two interactions, or escapes the material. In a detector, $\gamma$ decays produce three different peaks due to this interaction. Primarily, and most prominent is the full-energy

peak. At an energy $E_\gamma - m_e$, is the single escape peak, corresponding to one of the two photons escaping and not getting absorbed in the detector. If both photons escape, they will contribute to forming the double-escape peak at around $E_\gamma - 2m_e$ in the spectrum.

# 3 Scintillator detectors

Detecting nuclear decay products can be done using different instruments, mostly using detector technology. Detectors are pieces of equipment that exploit the mechanisms behind matter interaction, such as the $\gamma$ interaction mechanisms mentioned in the previous section, to produce easily read, stored and analyzed signals proportional to the energy of whatever was detected. One such type of detector is the scintillator detector, consisting of a scintillating material and a light readout sensor. A scintillator is a collective term for different materials where ionizing radiation is converted to photons. This means that the material has some internal mechanism that cause the material to produce light from ionizing radiation, as well as a transparency to the light it produces itself. There are many different kinds of material that suit this description and can be grouped into two major categories; organic- and inorganic scintillators.

Organic scintillators are typically plastics, liquids or glass. Plastic being the most common in use for larger detectors as they have low material cost and easy to produce and process in large amounts. The plastic scintillators are made up of a transparent host material, some kind of plastic, as well as some organic molecule capable of scintillation.

Inorganic scintillators are typically specially grown crystals, designed for their use in scintillator detectors. The crystals are more technologically challenging to produce than the organic counterpart, making them less suitable for large detectors. The high density and atomic numbers of inorganic crystal scintillators make them more suitable for use in $\gamma$- or X-ray detection.

## 3.1 Scintillation mechanics

There are many different mechanisms involved in the scintillation process. Theoretical descriptions of these are still an ongoing problem. One popular approach to the description of scintillation mechanics is the multiscale approach proposed by Vasil'ev and Getkin [2]. This approach suggest a series of interconnected processes that can run in parallel. The processes of relaxation of electronic excitations can be divided into five qualitative stages.[3]

The first step, is the electronic excitation. As high energy incident radiation interacts in the scintillator it creates deep holes and hot electrons. These produce secondary excitations by inelastic electron scattering, and auger processes as electrons recombine with the deep holes. These processes continue until all electrons have energies smaller than the electron-electron scattering threshold around 2 times the bandgap energy $E_g$ and all the holes created are located in the valence band.

For the second stage, the electrons and holes produce phonons via thermalization of the two. This leads to electrons in the bottom of the conduction band and holes in the top of the valence band with low kinetic energies. Through interactions with defects and impurities in the scintillator material excitations are localized in the third step. This can form self-trapped excitons (STE) and self-trapped holes ($V_k$) producing phonons. This localization step can be the cause of defects by displacing the atoms within the material, causing permanent changes in the scintillator.

For the final two stages the various interactions between the excitations take place, including the recombination of the electrons at the bottom of the conduction band with the holes at the top of the valence band as excitons decay. This exciton decay is what leads to the scintillation photon emissions used in detector readout.

According to a review article on the scintillation mechanisms in inorganic scintillators by Henry Chen and the sources therein the exciton decay has five major channels [4]:

- Scattering: The excitons scatter off of point defects, dislocations or the surface of the crystal. Causing no luminescence.
- Radiative decay: Free or trapped excitons recombine, producing a photon.
- Disassociation: The excitons disassociate due to photon scattering, collision, ionizing or defect scattering.
- Trapping: If defects have large enough cross sections, the excitons can get caught.
- Self-trapping: STE or exciton-phonon coupling causing the pseudo-particle to occupy states that are below the conduction band of the crystal but not part of the acceptor and donor level created by any dopants. From here, the exciton has an additional three major channels of decay:
  - Luminescence; the electron-hole pair manage to recombine and produce a photon
  - Thermal spikes: the exciton decays into a burst of phonons.

– Transferring: jumping to another site on the lattice or into any of the states created by introducing dopants.

## 3.2 $LaBr_3$(Ce)

The primary subject of this thesis is the inorganic crystal halide lanthanum bromide ($LaBr_3$). While the crystal itself is not a good scintillation material, doping the $LaBr_3$ with cerium generates cerium-activator states in the band structure of the crystal. These activator states enables many great scintillator qualities for the material. The cerium-activation incorporates the *4f* and *5d* bands of the cerium into the band structure of the crystal, allowing for additional sites for excitations and de-excitations. This greatly increases the light yield and the principal decay time of the host crystal. Cerium-activated lanthanum bromide ($LaBr_3$(Ce)) offer fast decay times, emission wavelengths matching with the requirements of common photocathodes, and good energy resolution. A comparison, done by Alexiev et al [5], between the $LaBr_3$(Ce), the common scintillator detector NaI(Tl), another lanthanum-halide $LaCl_3$(Ce) and a cadmium-zinc-telluride (CTZ) semiconductor detector shows that the $LaBr_3$(Ce) offers a superior resolution to both the NaI(Tl) and $LaCl_3$(Ce). The resolution has been recorded as low as 2.6% for $^{137}$Cs, approaching the Poisson statistical limit for scintillators. The $LaBr_3$(Ce) crystal demonstrates great linearity, which is an important quality for scintillators used in detectors. This light yield of the scintillator is kept uniform over a large span of temperatures [6].

The lanthanum-halides come with a few drawbacks. Lanthanum has a 0.09% natural abundance of the isotope $^{138}$La. This isotope contributes with an intrinsic background radiation in the scintillator. Furthermore the hexagonal structure of the $LaBr_3$ crystal, together with poor thermal diffusivity and low fracture strength of the material, causes internal stress as the crystal cools down from high temperatures, making larger crystal structures more prone to developing cracks if not cooled down properly [7].

The great time resolution, fast decay times, and the low effect temperature has on the scintillation properties make the $LaBr_3$-crystal an excellent candidate for usage in nondestructive assaying and nuclear waste management. Of further interest for this use-case is the impact of high radiation doses, and how potential changes in the crystal due to the radiation will impact the measurements.

## 3.3 Light readout sensors

The scintillation-photons produced in the crystal are typically difficult to quantify directly. Instead, these are converted into currents or voltages that are proportional to the intensity of the produced photons. This light readout can be done using different types of sensors

that all have different mechanisms to convert the scintillation photons to current or voltage signals , with varying degrees of amplification and response fluctuations.

### 3.3.1 Photodiodes

The conventional photodiode (PD) has no internal gain and instead directly converts the scintillation photons to a number of electron-hole pairs. Photodiodes used with scintillation detection are typically PIN photodiodes, named after the three layers of semiconductors that make up the diode: A p-type layer, an undoped intrinsic layer and finally an n-type semiconductor layer. The photodiode is operated in a reverse bias connected to the outer p- and n-type layers. Incident light penetrates the usually very thin p-type layer, and ionize in the intrinsic layer, forming electron-hole pairs. The pair drift in opposite directions, inducing a small charge. This charge can be processed by a preamplifier and shaped into a suitable signal pulse.[6]

The photodiode has a great quantum efficiency compared to other light readout sensors as it does not rely on charge carriers overcoming the vacuum level barrier as devices using photocathodes do. On the other hand, the lack of gain in photodiodes results in very low amplitudes of the signals to the preamplifier. This leads to the PD being prone to noise. This noise primarily comes from three sources: Series noise from the preamplifier input, parallel noise, from the fluctuating leakage current, and the capacitance of the fully biased detector. These noise-sources are highly dependent on the size of the photodiode, limiting the surface of the scintillator material PD can cover.[6]

### 3.3.2 Avalanche photodiodes

Avalanche photodiodes(APDs) produces charge in the same way as in a conventional photodiode but contains an amplifying element. Introducing an additional p-type layer between the intrinsic region and the n-type layer typically referred to as the avalanche region. Electron-hole pairs formed in the intrinsic-layer, or drift region. Subsequently the electrons are accelerated towards the avalanche region where they collide with the lattice of the semiconductor layer. The kinetic energy is deposited in the lattice, causing the formation of additional electron-hole pairs via collision ionization. This causes an amplification of the signal in the APD compared to a conventional PD. [6]

A higher amplitude of scintillation signals, a greater signal-to-noise ratio and still maintaining the high quantum efficiency of the photodiode. All these qualities typically make the APD a more suitable candidate for use in scintillator detectors than conventional PIN photodiodes. The major downsides of the APD are the large temperature dependence in the gain, where an increase of temperature quickly lead to smaller and smaller gain. The

avalanche process also has stochastic element to it, causing the gain to fluctuate randomly causing further noise. [6]

### 3.3.3 Silicon photomultiplier

A popular approach to the APD is the Silicon photomultiplier (SiPM). Approaching the readout mechanics in much the same way. A grid for connected avalanche photodiodes are connected in series to their own quenching resistor. This grid is connected in parallel at a voltage such that every pixel is slightly above its breakdown voltage. The grid-structure of the SiPM offers a greater gain compared to a single APD. But the same close-lying structure of the SiPM comes with an additional issue. Discharges from a single cell, from incident photons, can cause discharges in near-lying cells. Photons generated in the avalanche region of a cell can either interact promptly, in the avalanche region of a neighboring cell. Or it can produce a charge carrier that diffuse into a neighboring cells avalanche region, causing a secondary delayed avalanche. Both these interactions increase the perceived incoming photon flux, causing excessive noise.

### 3.3.4 Photomultiplier tubes

A common approach for converting the scintillation photons into electrical signals is the photomultiplier tube (PMT). The PMT has two elements: First, the photosensitive layer photocathode. Secondly, the electron multiplication structure.

Photons incident on the photocathode excites electrons in the valence band of the material. The excited electrons diffuse toward the surface of the material. If the absorbed photon energy $h\nu$ is enough, the excited electrons can overcome the vacuum barrier level and be emitted from the material. The ratio of incoming photons and outgoing electrons to the material in this process is given by

$$\eta(\nu) = (1 - R)\frac{P(\nu)}{k} \cdot \frac{1}{1 + 1/kL} \cdot P(s) \tag{3}$$

where $R$ is the reflection coefficient, $k$ is the full absorption coefficient of the photons, $P(\nu)$ is the probability of light absorption exciting the electrons above the work function, $L$ is the mean escape length of excited electrons and $P(s)$ is the probability of electrons excited to the surface to be released into the vacuum [8]. The majority of these coefficients are optimized by selecting the proper material when constructing the photocathode.

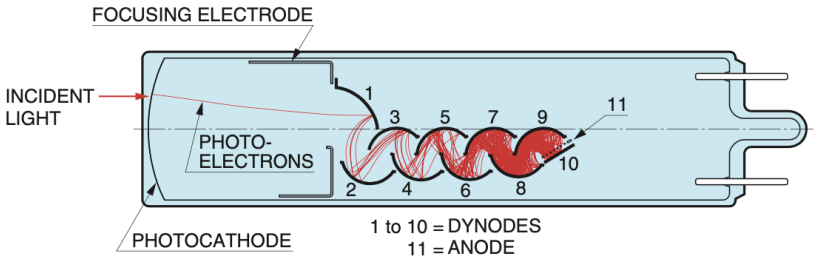


Figure 3: Illustration of of a photomultiplier. Taken from [8]

Electrons emitted from the photocathode are accelerated and focused toward the first dynode of the electron multiplier using electrodes, as seen in Figure 3. A high potential difference between the cathode and a final anode continues to accelerate the electrons between subsequent dynodes. Each dynode is connected to a voltage divider, setting up a voltage gradient across the electron multiplier. Electrons colliding with a dynode cause the emission of secondary electrons causing an amplification of the initial current up to $10^8$ across the entire electron multiplier. Finally the amplified current reaches the anode. The secondary electrons are gathered, outputting an electrical pulse that is proportional to the initial incident scintillation photons.

## 3.4 Detectors

Mounting a light readout sensor to a scintillating crystal allows it to be used as a detector. Incoming $\gamma$ radiation deposit its energy in the sensitive region of the scintillation material, while giving a proportional response in the form of scintillation optical photon intensity. These scintillation photons are incident to the light readout sensor that conversely turn the scintillation photons into signals of current or voltages. The amplitude of the signals are proportional to the intensity of photons, and are easily readable by modern instruments. Using an analog- to digital converter(ADC) and histogramming the digitized signal amplitudes allows for the visualization of spectra such as Figure 2.

### 3.4.1 Resolution & Fano Factor

The different mechanisms discussed in the above sections that take place in the process of converting the $\gamma$-decay to readable signals present themselves in the spectra differently. These factors cause the $\gamma$-decay energies to distribute as a Poisson distribution. An important characteristic of a ionizing radiation detector is the energy resolution of the detector. This resolution is given by the width of energy in the peak relative to the energy of the decay

$$R = \frac{\Delta E}{E}. \tag{4}$$

The variance of the Poisson distribution in detector signals is given by the mean number of events:

$$\sigma^2 = J. \tag{5}$$

The number of events can be related to the energy of the decay $J = E/w$. Where $w$ is the energy necessary to produce an ionizing event in the material. At the full width half maximum (FWHM) of the peak, we find the resolution:

$$R = 2.35\frac{\sqrt{J}}{J} = 2.35\sqrt{\frac{w}{E}} \tag{6}$$

Where the factor 2.35 is the full width half maximum of a Gaussian distribution, which can also be used in calculating the resolution of a peak

$$R_{FWHM} = \frac{FWHM}{E}. \tag{7}$$

Unfortunately the many mechanisms at play in the process disrupt the Poisson statistics behind the above assumption. The processes are not independent from one another and cause the variance to differ from what a statistical prediction would find. In [9], the so-called 'Fano'-factor is introduced. This typically experimentally determined factor relates the actual variance of the detector response, to that of an Poisson distribution.

$$\sigma^2 = FJ = F\frac{w}{E}. \tag{8}$$

$F$ is a result from all the different fundamental processes taking place and is difficult to determine theoretically. With the Fano factor taken into account Equation 6 is given by

$$R = 2.35\sqrt{\frac{Fw}{E}}. \tag{9}$$

Other than the internal mechanisms of the detector, external factors such as electrical noise also have an effect on the experienced resolution. Assuming these factors are independent to one another, the effect they have on the measured FWHM can be separated:

$$\sigma^2 = \sigma^2_{detector} + \sigma^2_{electrical} + ... \tag{10}$$

Where each term is a different source of variation from the true peak.

# 4 Nondestructive assaying

Nondestructive assaying (NDA) is a generic term describing measurement techniques that aim to confirm the isotropic composition and quantity of nuclear material without destroying the subject. Typically by measuring the radioactive decay emitted by the subject of the assaying. Compared to destructive analysis, where similar goals are achieved using destructive chemical procedures on samples of the material, NDA typically reduces the exposure to radiation, minimizes costs and takes less time [1].

Spent nuclear fuel may pose a large risk to humans, animals and the environment around it if not stored and handled properly. Addressing this risk, a long term solution by burying it deep in Swedish bedrock has been proposed [10]. This proposition involves multiple temporary storage solutions, and when the spent nuclear fuel is ready to be transported and handled properly, a final storage. These steps require NDA techniques to be employed. As described in a technical report by Swedish Nuclear Fuel and Waste Management Company [10] initial handling of the spent nuclear fuel must be done in close proximity to the producer of said fuel. The spent fuel must be given sufficient time for the decay power to decrease to levels low enough for transportation and deposition in the final repository. To maximize the storage space of the spent nuclear fuel, limited by the decay heat produced by the radioactive material it is of importance to determine the remaining activity of the spent fuel. Proposed in [11] is a method describing how to measure the activity of $^{137}$Cs in spent nuclear fuel. This involves first calibrating using a similar source with a well-known activity. From this the activity

$$A_i = \frac{I_i}{\varepsilon_i} \tag{11}$$

of a source can be determined. Here, $\varepsilon_i$ describes the absolute efficiency of the detector used in measurement, and $I_i$ the measured intensity of $\gamma$-decay.

# 5 Experimental setup

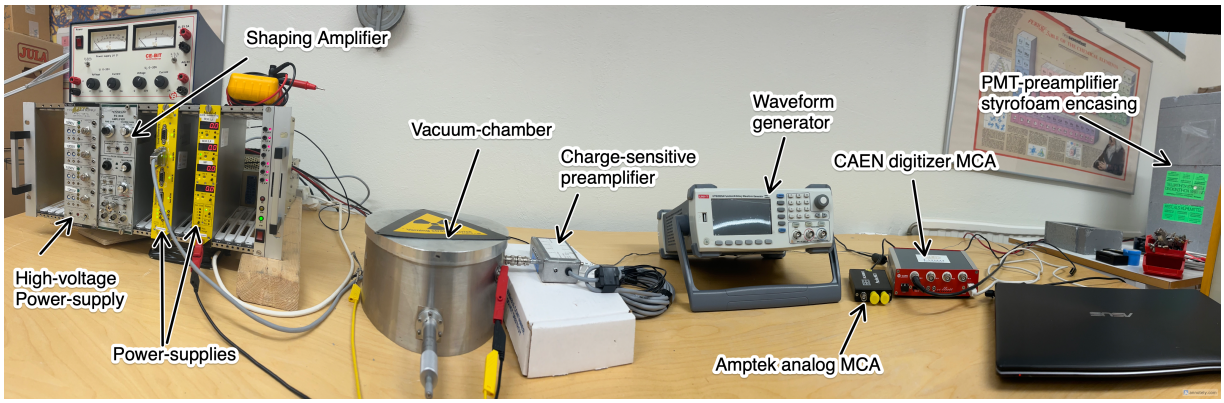


Figure 4: Image of the experimental setup, with annotations for the different components. In the image, the setup is connected for measurements using the PMT housed in the styrofoam enclosure (far right)

In performing the measurements, a set of different tools and electronics are used. Among these are the three inorganic crystal scintillators, two of which are seen in Figure 5, that are compared.

Figure 5: Two of the scintillators used in measurements. On the left is the irradiated $LaBr_3$, and on the right the comparative NaI(Tl)

## 5.1 Radiation-damaged $LaBr_3$(Ce) Scintillator

The subject of the thesis is a $35\varnothing \times 50$ mm cesium-activated lanthanum bromide scintillator crystal shown on the left in Figure 5. This crystal has been exposed to approximately 9.8 kGy of $\gamma$- and neutron radiation. Visibly the scintillator has sustained multiple cracks. The largest of the fractures split the entirety of the crystal volume along its cylindrical axis. To mitigate the possibility of getting double-peaks and odd signal signatures due to the main fracture, the smaller of two sub-volumes is blocked off and no longer in use

during the scintillation measurements. However, smaller fractures are still visible in the remaining volume. Beyond this no visible alterations of the $LaBr_3$ crystal are present. Due to the hygroscopic sensitivity of the crystal, it is housed in a thin metal cylindrical casing with glass window on one of the ends.

## 5.2 Comparative NaI(Tl) Scintillator

For comparison of the measurements done with the irradiated $LaBr_3$ scintillator crystal, a commonly used NaI(Tl) crystal is used. The $35\varnothing \times 30$ mm NaI(Tl) crystal, seen on the right in Figure 5, is smaller than the original $LaBr_3$ volume. A small fracture is visible on the surface of the crystal. Similarly to the radiation-damaged $LaBr_3$ crystal, the NaI-crystal is housed in a thin metal cylindrical casing with a window in one of the cylinder caps.

## 5.3 Reference $LaBr_3$(Ce) Scintillator

As a second comparative measurement, a $LaBr_3$ crystal of similar origins as the radiation-damaged $LaBr_3$ was used. This scintillator crystal was already in use for different experiments, and was encased in a thick lead and wolfram box to reduce background of the measurement and collimate incoming $\gamma$ radiation.

## 5.4 Detector readout chain

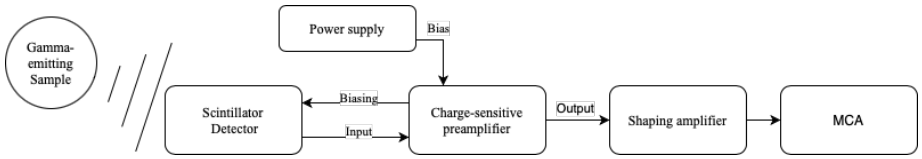


Figure 6: Sketch of a typical analog detector readout chain used for $\gamma$ spectroscopy.

To process the scintillator detectors scintillation response and produce an emission spectrum of a radioactive sample, several components need to be used. Figure 6 illustrates the components that are employed in such a chain. For the purpose of this thesis, both an analog multichannel analyzer(MCA) as well as a digitizer are used. The digitizer taking the places of both the shaping amplifier and the MCA in the chain, combined into one component.

### 5.4.1 Charge-sensitive preamplifier

The current pulse generated by the light readout sensor is typically too small to be sensed directly. Using a charge-sensitive preamplifier to act as an interface between the detector

and the processing chain. The preamplifier produces a step in voltage that is proportional to the current pulse $Q$. The voltage step produced is

$$V = \frac{Q}{C}, \tag{12}$$

where $C$ is the input capacitance. For this reason, to avoid exacerbating the signal-to-noise ratio of the pulse, the distance between the detector unit and preamplifier is minimized. Long cables running between the two will cause the inherent capacitance of the wires to degrade the signal-to-noise ratio and final energy resolution.

The power supply that is used for biasing the light readout sensor to the appropriate voltage is usually connected via the preamplifier as illustrated in Figure 6.

### 5.4.2 Shaping amplifier

The voltage step pulse generated by the preamplifier is a tail pulse with a long decay time. The long tail will cause pile-up as subsequent signals land on the tail and present an amplitude equal to the superposition of the signal as well as the tail, no longer proportional to the initial scintillator response. Therefore shaping the signal is necessary to be able to read out individual $\gamma$-emissions from a high activity sample. The most common way of using analog electronics in shaping a signal is the CR-RC pulse shaping method [12]. CR-RC shaping sends the signal through a differentiator, filtering the low frequencies, and a integrator which filters the high frequencies.

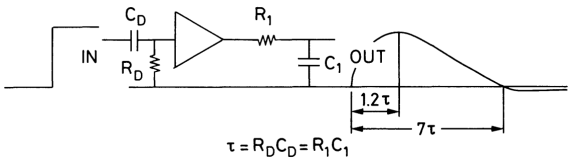


Figure 7: CR-RC pulse shaper, showing the difference between an idealized step-function pulse generated by the preamplifier, and the resulting pulse shape after CR-RC shaping. Taken from [12]

This greatly improves the signal-to-noise ratio and outputs a smooth unipolar pulse with a much shorter tail than what is produced in the preamplifier. However, due to the differentiation of the finite-length tail pulse in the RC-circuit, the shaped pulse undershoots the baseline restoration. This causes a disparity between the baseline before and after the shaped pulse, causing subsequent pulses to have an amplitude defect. To fix this undershoot, a pole-zero cancellation circuit is used at the end of the shaping amplifiers operation. By adding a variable resistor in parallel to the capacitor in the CR-circuit, the undershoot can be adjusted until negligible.

As the name suggests, the shaping amplifiers also contribute by adding an adjustable

amplification to the resulting pulse. This adjustable gain allows for varying the output of small pulses to better match the input range of the ADC. For the measurements presented in this thesis, a Tennelec TC-244 nuclear instrumentation module was used as the shaping amplifier.

### 5.4.3 Multichannel analyzer

The MCA is a device that is used to record and sort the amplitudes of incoming pulses. The amplitude of the pulses are digitized using an ADC, and placed in channels, or bins, representing the input voltage range of the MCA. The number of available channels is called the conversion gain of the MCA. The ADC central to the MCAs functionality typically has strict requirements for the rise time and shape of the incoming signals, which further emphasizes the importance of the shaping amplifier.

When doing the measurements two different MCAs were used. Along with the classical analog shaping and amplifying, an Amptek MCA-8000D multichannel analyzer [13] was used. This device samples at a 100 MHz rate and has a conversion gain of 8000 channels for input ranges 0-10 V or 0-1 V.
The second MCA is a CAEN DT5781 Quad Digital Multi Channel Analyzer [14]. The DT5781-digitizer replaces both the shaping amplifier as well as the MCA in the chain, providing its own shaping parameters. The digitizer samples the output pulses of the preamplifier and converts them to a continuous data stream at a rate of 100 MHz. These pulses are digitally shaped with a trapezoidal filter, known as moving window deconvolution. This filter utilizes a recursive algorithm to generate a symmetric trapezoidal pulse from the input tail pulse, produced by the preamplifier [15].

Both of these MCA connect directly to a computer using a USB-interface, and are controlled by their respective software.

# 6 Method

A total of 3 different $\gamma$-emitting samples were used, $^{137}$Cs, $^{22}$Na, and $^{60}$Co. As well as three different light readout sensors, to determine if there is any difference in scintillator response and enlarge the data pool. The sensors used were the Hamamatsu S3590-05 photodiode [16], Hamamatsu S13360-3025CS silicon photomultiplier[17], and the PHOTONIS XP2262(B) photomultiplier tube[18]. Two of the aforementioned crystals, the damaged $LaBr_3$ and the NaI(Tl) were mounted to different light readout sensors whose functionality is described in subsection 3.3. For the PD and the SiPM: the light readout sensors were sequentially mounted using Permacol RTV 615 casting resin, fastening the sensors

to the window of the crystal. This resin acted like a optical adhesive between the crystal and sensor, allowing for minimal refraction and reflections of the scintillation photons. The remaining surface of the crystal window was covered with a reflective film, so as to prevent light escaping from the crystal without producing a signal in the PD. The detector was then placed in a experimental chamber, serving as a small darkroom for taking measurements. A $\gamma$-emitting sample was placed at a short distance from the closed cap of the crystal casing. Adjusting the gain, threshold, and on the DT5781 the trapezoidal filter between swapping light readout sensors as to make sure the best possible resolution with the setup was achieved. This measurement process was repeated for the different permutations of samples and light readout sensors.

The photomultiplier tube was mounted to the crystal using Saint-Gobain Crystals BC-630 Silicone grease [19], to maximize optical contact between crystal- and PMT windows. The PMT was then enveloped in mu-metal, shielding the sensitive dynodes from electromagnetic interference (EMI). The detector was then connected to a preamplifier made for accommodating PMTs and the rest of the detector chain. The detector and the preamplifier were enclosed in styrofoam with a small hole for collimating $\gamma$-emissions. To further collimate the samples, a lead casing with a small exit lined up with the hole in the styrofoam enclosure was used to contain the sample being measured. Similarly this procedure was repeated for all permutations of the two crystals and three samples.

All above procedures were tested using both the Amptek MCA-8000D multichannel analyzer, and the CAEN DT5781 MCA to get the best possible results using the built detector chain. $\gamma$-emissions were gathered and recorded for different times based on the activity of the sample, such that the purely statistical deviation from the $\gamma$-decay energy were minimized in the spectra. Recording continued until the expected $\gamma$-peaks presented as close to gaussian distributions as possible.

For the third scintillator crystal specified in subsection 5.3 measurements were only done using the CAEN DT5781 MCA. Mounted on the crystal were high-grade SiPM and electronics. Due to the heavy collimation setup around the scintillator and lack of an active enough sample, detector measurements of $^{22}$Na were excluded.

To determine the intrinsic resolution of the scintillators, a well-defined pulse generated using a Uni-Trend UTG2025A waveform generator [20] fed straight into the DT5781 MCA was used. The histogramming of the well defined pulse allows for determining the FWHM that is inherent in the digitizer. Since this uncertainty is separate from the response of the actual detector, the two are separable as described in Equation 8. Using this separability, the energy resolution and the Fano factor intrinsic to the scintillator detector of the can

be calculated.

# 7 Results & Analysis

Measurements done with both the PD as well as the SiPM yielded no visible results. This likely due to a low light output of the irradiated crystal, yielding no discernible $\gamma$ energy peaks attempts to measure spectra. The PMT-measurements on the other hand yielded viable spectra. The main peaks of each $\gamma$-source; 511 keV, 661.7 keV, 1173.2 keV and 1332.5 keV for $^{22}$Na,$^{137}$Cs, and the double peaks of $^{60}$Co respectively, were fit assuming an approximately gaussian distribution of the counts. Assuming a linear background, the gaussian distribution of each peak was used in accordance with Equation 7 to calculate the resolution of each permutation of detector and $\gamma$-peak.

Table 1: Spectral resolution measurements using the photomultiplier tube, given in percent. The presented measurements were done using the DT5781 as described in section 6

| Sample / Detector | $^{22}$Na E=511.0 keV | $^{137}$Cs E=661.7 keV | $^{60}$Co E=1173.2 keV | $^{60}$Co E=1332.5 keV |
|---|---|---|---|---|
| Irradiated $LaBr_3$(Ce) | 7.234(9)% | 6.193(1)% | 4.851(32)% | 3.445(28)% |
| $LaBr_3$(Ce) | N/A | 3.261(1)% | 2.522(6)% | 2.459(6)% |
| NaI(Tl) | 11.20(3)% | 10.02(3)% | 7.600(500)% | 4.900(600)% |

Typical values for a $LaBr_3$(Ce)-scintillator places the resolution for the 661.7 keV $^{137}$Cs-peak around 3.1% [21]. This is comparable to the results measured for the undamaged detector where the resolution for the same peak was measured to be 3.261(1)%. This is within the range of values provided for the detector before radiation damage [Linus Ros, private communication]. These measurements show a resolution around 3-4% for a 661.7 keV peak.

The irradiated LaBr-scintillator as expected resulted in significantly worse resolution peaks. The relative difference:

$$\frac{R_{rad} - R_{ref}}{R_{ref}} \tag{13}$$

where $R_{rad}$ and $R_{ref}$ are the resolution measured on the irradiated- and the reference LaBr-scintillator detectors respectively, shows the resolution degraded with an average of 74.1% after the damage. The $^{60}$Co 1173.2keV peak having an increase in resolution as high as 92.3(13)%. Despite the degradation of the irradiated LaBr-scintillator, it still outperforms the NaI(Tl)-scintillator in both resolution and apparent yield. As visible in

Figure 8a-c, the signal-to-noise and signal-to-background ratios of the irradiated LaBr (blue) are significantly better than the NaI (green).

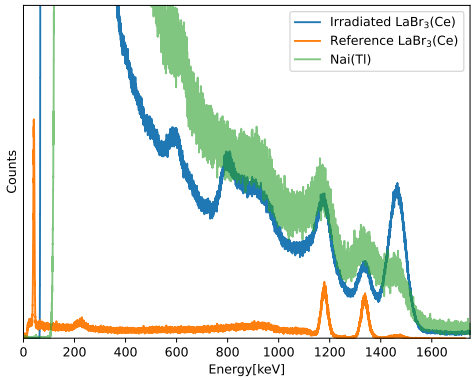


(a) $^{60}$Co.

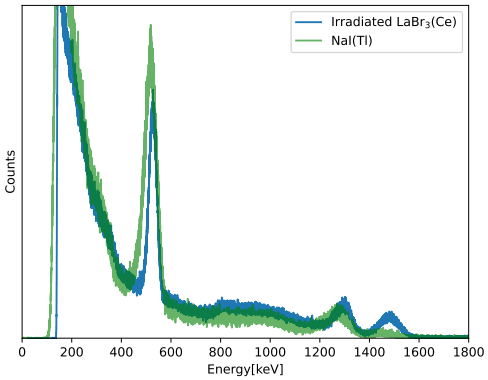


(b) $^{22}$Na.

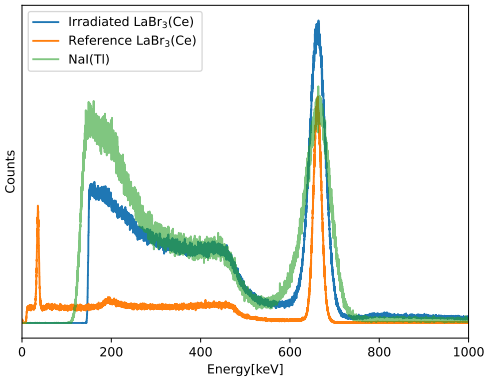


(c) $^{137}$Cs.

Figure 8: $\gamma$-ray energy spectra as measured for three standard calibration sources - $^{60}$Co (a), $^{22}$Na (b) and $^{137}$Cs (c). Counts of the different measurements have been adjusted by some factor to improve visibility of the relative performance of the scintillator detectors.

The variance in counts for neighboring channels for the NaI-spectra, especially the $^{60}$Co-spectra in Figure 8a also presents as a significant difference from the irradiated LaBr scintillator. This feature is reflected in the error of the measured resolution, which is higher for the NaI-detector than either of the other two. The same comparison is difficult to make between the NaI(Tl) or the irradiated $LaBr_3$ and the reference LaBr-scintillator, as the measurements done with that detector was done under very different conditions.

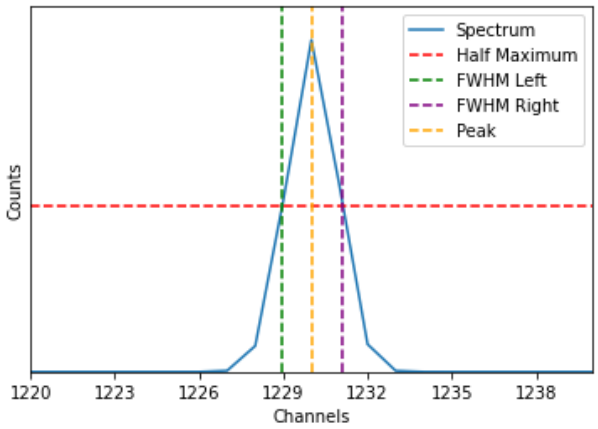


Figure 9: The FWHM of a well defined pulse as measured using the CAEN DT5781 MCA.

By measuring the FWHM of a well-defined pulse as plotted in Figure 9, Equation 10 is used to estimate the intrinsic resolution of the irradiated and reference $LaBr_3$-scintillators. The intrinsic resolution of the $^{137}$Cs 662 keV-peak for the irradiated LaBr-scintillator is calculated to be 6.220(3)%, and 3.25(1)% for the reference LaBr. For a $LaBr_3$-scintillator with a light output of around 63000 photons/MeV [22], the mean ionization energy $w$ can be estimated to $w = \frac{10^6}{63000} \approx 15.9$ eV/photon. From this and the intrinsic resolution, the Fano factor $F$ before and after the irradiation process can be estimated. Assuming the mean ionization energy is constant before and after irradiation, the Fano factor is given by, from Equation 8,

$$F = \frac{\sigma_{stat} w}{E_{137Cs}}. \tag{14}$$

The calculated Fano factor is approximately 0.42 for the irradiated detector and 0.22 for the reference.

# 8 Discussion

The visual damage done to the LaBr-scintillator due to excessive exposure to radiation appears to be limited to the large fractures sustained. Without deeper insight into the irradiation procedure and the following resting period, it is not possible to discern whether these fractures appeared as a direct result of the radiation, or a result of uncontrolled cooling of the crystal. The latter of the two possible causes being the better and more easily controlled option. If the fractures in the crystal were caused by rapid cooling of the scintillator after irradiation, proper procedures would enable $LaBr_3$-detector units to be exposed to heavy radiation without sacrificing the volume of the crystal. Despite the reduction in volume of the LaBr-crystal, studies on the performance of large $LaBr_3$ scintillators show no significant degradation of the relative performance, light output, linearity, or the energy resolution for different sizes of crystals [21]. This differs from the NaI(Tl)

where size has a significant impact on the detector qualities. However, the reduction in volume for the $LaBr_3$ scintillator will cause a decrease in the geometrical efficiency of the detector possibly causing further exacerbation of the signal-to-noise ratio. It is not clear from this experiment if the existing fractures and subsequent asymmetry of the volume has had an effect on the measured resolution of the $\gamma$-peaks.

The difference between the two experimental setups utilizing the irradiated LaBr- and NaI-detectors, and the reference LaBr-detector is clear from the difference in background counts measured between the two. While the former has a clear lower limit, due to excessive noise, the reference LaBr (orange in Figure 8a and 8c) has significantly lower background. This excessive background and noise hinders the visibility of low-energy features in the spectra such as the 32 keV $^{138}$Ba x-ray due to the inherent $^{138}$La present in the LaBr-scintillators. The excessive background and noise being present, and similar, in both the irradiated LaBr- and the NaI measurements indicates that this is a contribution of the experimental setup rather than an effect of the irradiation. This difference in background and noise may also be a contributing factor to the measured difference in resolution. It may also have played an important part in the separation of uncertainties when calculating the intrinsic resolution and Fano factor of the two LaBr-scintillator detectors. While the uncertainty caused by the MCA in particular was subtracted, other sources of noise such as the ones in the spontaneous electron emission due to the temperature of the PMT [23], the preamplifier, electromagnetic interference between these junctions. This remaining noise impacts the calculated Fano factor negatively, causing a larger variance in the signal from sources that are not intrinsic to the structure of the scintillator itself. While both the irradiated and the reference scintillators display sub-Poissonian variance in the signals, the irradiated LaBr has nearly twice the Fano factor of the reference detector. This shows the impact of the 9.8 kGy radiation that the scintillator was exposed to, causing a significant degradation of the detector performance. This could have been caused by a multitude of different structural changes. The high kinetic energy transferred to the scintillator in this radiation process leads to defects and displacements in the crystal structure of the LaBr. This increases the cross section for trapping of excitons, as well as increasing the scattering within the crystal and the disassociation of the excitons. These interactions enhance or introduce new avenues for the energy to escape through means other than luminescence, causing a higher Fano factor and a larger variance in the scintillator response.

Comparing the results obtained in this work to similar studies such as [24] and [25].In [24] a resolution degradation of approximately 50% the original resolution after a $\gamma$-dose of 11 kGy is measured. The same study also found that recovery time between irradiation and the following measurement allows for the resolution to improve. Similarly [25] measures a significant degradation in light yield and resolution for the $LaBr_3$-scintillator

following exposure to large doses of radiation, measuring as much as a 170% degradation of resolution after a 10 kGy dose. The most significant degradation was found to occur within the first Gy of irradiation. A sharp decrease in light yield also contributes to having a larger background, as the peaks no longer being as prominent. The measured resolution degradation of 74.1% in this thesis, given a long recovery period between irradiation and measurement, seems to agree reasonably well with similar experiments.

# 9 Conclusion & outlook

The 9.8 kGy irradiation process has caused clear degradation of the detector qualities of the $LaBr_3$ scintillator. Comparisons show an average degradation of 74.1% in resolution for the $\gamma$ peaks measured with a radiation-damaged scintillator crystal versus a normal functioning one, further reflected in the nearly double Fano factor calculated for the irradiated. In addition to the degradation in resolution, the scintillator has suffered multiple fractures which further compromise its functionality. These factors all put into question the viability of the $LaBr_3$-scintillator detector in NDA-applications. The decay-heat that the detector is intended to measure may, in high doses, contribute to the degradation of the detector itself. The degradation found for the irradiated LaBr-detector may also serve as valuable experimental data in improving future simulations of such scintillators in high radiation scenarios.

Further characterization of the radiation-damaged crystal may be necessary, determining possible degradation in the absolute light output and linearity of the scintillator response. It is also necessary to investigate the reason behind the large fractures in the crystal. Similar degradation studies of the scintillator such as [24] and [25] do not mention any issues with structural integrity after exposure to radiation. If this, as previously mentioned, was caused due to the fast cooling of the crystal, further studies going into how to prevent and optimize the cooling process should be conducted. Such studies may bring greater insight into the use of this type of scintillator detector in the area of NDA and if the degradation in quality over time outweighs the cost of the detector. If not, the detector will require heavy shielding or increased distance and time during NDA, such that the effective dose on the detector is minimized, resulting in less efficient usage.

# References


[1] W. H. Geist, P. A. Santi, and M. T. Swinhoe, eds., *Nondestructive Assay of Nuclear Materials for Safeguards and Security*, Second Edition (Springer Nature Switzerland, 2024).

[2] A. N. Vasil'ev and A. V. Gektin, IEEE Transactions on Nuclear Science **61**, 235 (2014).

[3] P. Lecoq, A. Gektin, and M. Korzhik, *Inorganic Scintillators for Detector Systems* (Springer International Publishing, 2017).

[4] H. Chen, in Hard x-ray, gamma-ray, and neutron detector physics xxiv, edited by N. J. Cherepy, M. Fiederle, and R. B. James (Oct. 2022), p. 4.

[5] D. Alexiev et al., IEEE TRANSACTIONS ON NUCLEAR SCIENCE **55**, `10.1109/TNS.2008.922837` (2008).

[6] G. F. Knoll, *Radiation detection and measurement*, Fourth Edition (John Wiley Sons Inc, Sept. 2010).

[7] P. R. Menge, M. Bush, L. Wilson, and B. S. Bacon, IEEE Transactions on Nuclear Science **60**, 1039 (2013).

[8] Hamamatsu Photonics, *PHOTOMULTIPLIER TUBES Basics and Applications*, tech. rep. (Hamamatsu Photonics K.K., 2017).

[9] U. Fano, Physical Review **72**, 26 (1947).

[10] Svensk Kärnbränslehantering AB, *Design and production of the KBS-3 repository*, tech. rep. (Svensk Kärnbränslehantering AB, Dec. 2010).

[11] M. Bengtsson et al., Nuclear Technology **208**, 295 (2022).

[12] W. R. Leo, *Techniques for Nuclear and Particle Physics Experiments* (Springer Berlin Heidelberg, 1994).

[13] *MCA8000D User Manual*, Amptek ().

[14] *User Manual UM3188 DT5781 Dual/Quad Digital MCA*, CAEN (Apr. 2011).

[15] V. T. Jordanov and G. F. Knoll, Nuclear Instruments and Methods in Physics Research Section A: Accelerators, Spectrometers, Detectors and Associated Equipment **345**, 337 (1994).

[16] *Si PIN Photodiode S3590-01/-05/-08: Large area sensors for scintillation detection*, Hamamatsu Photonics (2001).

[17] *S13360 series: MPPCs for precision measurement*, Hamamatsu Photonics (2024).

[18] *XP2262 product specification*, Photonis (1998).

[19] *Technical data sheet PERMACOL RTV 615 A/B*, Permacol industrical adhesives (No year given).

[20] *UTG2000A User Manual*, Uni-trend technology (No year given).

[21] P. R. Menge et al., Nuclear Instruments and Methods in Physics Research Section A: Accelerators, Spectrometers, Detectors and Associated Equipment **579**, 6 (2007).

[22] K. Alzimami et al., Journal of Radioanalytical and Nuclear Chemistry **278**, 755 (2008).

[23] H. O. Meyer, EPL (Europhysics Letters) **89**, 58001 (2010).

[24] W. Drozdowski et al., Radiation Measurements **43**, 497 (2008).

[25] Z. Li et al., Asian Journal of Chemistry **26**, 4439 (2014).